A diamond gammavoltaic cell utilizing surface conductivity and its response to different photon interaction mechanisms

G.R. Mackenzie [a, *], S. Kaluvan [a], P.G. Martin [a], C. Hutson [a], T. Connolley [b], M. Cattelan [c, d], H. Dominguez-Andrade [a], T.L. Martin [a], N.A. Fox [a, c], T.B. Scott [a]

[a] School of Physics, University of Bristol, Bristol, BS8 1TL, UK
[b] Diamond Light Source, Harwell Science and Innovation Campus, Didcot, Oxfordshire, OX11 0DE, UK
[c] School of Chemistry, University of Bristol, Bristol, BS8 1TL, UK

ARTICLE INFO

ABSTRACT

This paper presents a diamond gammavoltaic cell—a solid-state device that converts gamma radiation into electricity—with a novel design and promising capabilities. Gammavoltaics pose a unique challenge among radiovoltaics due to the highly penetrating nature of gamma rays. To adapt existing radiovoltaic and dosimeter designs by increasing their thickness risks throttling the flowing current due to an attendant increase in series resistance. The presented design partially decouples this relationship by creating a low-coverage hydrogen-terminated collection volume around the device, exploiting the transfer doping effect. This paper proves that hydrogen termination is necessary for the gammavoltaism exhibited. Data are then presented from current-voltage curves taken using synchrotron radiation over the range 50-150 keV. A drop in the series resistance over the range is discovered and linked to the transition from the photoelectric effect to Compton scattering. The cell produces an open-circuit voltage $V_{OC} = 0.8$ V. Its short-circuit current I_{SC} and maximum power P_{max} are found to also depend on photon energy, reaching maxima at ~150 keV, where $I_{SC} > 10$ μA and $P_{max} > 3$ μW, normalized in flux to 2×10^{11} γ.s^{-1}. Groundwork is hence laid for developing this type of cell for micropower applications.

© 2021 Published by Elsevier Ltd.

1. Introduction

As a field, photovoltaics remains synonymous with solar photovoltaics. However, the same effect is produced for photon energies outside of the visible range, and research has sporadically appeared to investigate the potential of photovoltaics for much higher photon energies: gammavoltaics. Other radiovoltaic devices, namely alphavoltaics [1] and betavoltaics [2–6], which generate electricity under illumination from alpha and beta particles, respectively, are often intended for use as portable micropower devices with incorporated radioisotope sources. Gammavoltaic devices are different, as the shielding requirements of gamma isotopes are much greater. Therefore, gammavoltaic devices are better suited for deployment into existing gamma fields. While this limits the applicability of gammavoltaics compared to other

radiovoltaics, it also provides an advantage in that no isotope sourcing or handling is necessary for the creation of devices. The device is made and then brought to the often-substantial source. In nuclear waste stores, for example, where simple measurements of temperature and humidity are desired (i.e. measurements with low power requirements), ambient gamma dose rates are around 100 Gy/h, and the canister surface dose rates are estimated to be as high as 1,200 Gy/h.[e] In such places, micropower sensors would provide much greater information density about the interior, and hence, lower the risk of the store. As such, as for other radiovoltaics, micropower outputs are the current goal for gammavoltaics. When gamma rays hit a gammavoltaic, the device produces current through electron-hole pair generation and separation, with separation proceeding due to a built-in voltage, as in solar photovoltaics. Gamma photons (defined here as any photon emitted by a nucleus rather than by an energy range) can have energies in the visible range [7]. But typically, they have between one-thousand

---

* Corresponding author.
 E-mail address: gm12172@bristol.ac.uk (G.R. Mackenzie).
[d] Present address: Elettra − Sincrotrone Trieste S.C.p.A., Strada Statale 14 − km 163,5 in AREA Science Park, 34149 Basovizza, Trieste, Italy.

[e] Sellafield Ltd., private communication, 2020.

and one-million times the energy of solar photons, the vast majority of which have an energy less than 5 eV under standard AM1.5 domestic conditions [8]. Therefore, the number of electron-hole pairs generated per photon can be larger, but the photons can also be far less likely to interact with the active volume of the device (c.f. the cross-section values in Ref. [9]).

There is not yet a commercially-available gammavoltaic cell, nor has one been demonstrated that can provide long-term power. This is largely a material issue. Silicon photovoltaic cells, whether used as direct conversion devices [10,11] or in tandem with scintillator layers [12,13], can be used as gammavoltaics but are susceptible to damage. Other researchers have taken a different approach, using single-crystal methylammonium lead triiodide [14–17]. Degradation has been observed, but devices have withstood dose rates of 100 Gy/h. These devices, being composed of a lead-containing perovskite, are particularly elegant in being highly absorbing direct conversion devices. However, at the time of writing, they still require the application of a small (<1 V) bias and are, in that sense, still detectors rather than standalone voltaics. Liakos, along with a theoretical treatment of scintillator-based gammavoltaics for Co-60 [18], has also modeled the effectiveness of using Th-229, which emits gamma rays with very low energies [7], as a safe in-built radioisotope [19]. To our knowledge, although the studies were promising, these devices were never made. This paper presents a device made from diamond. Due to the strength of the sp^3 C–C bond in diamond (3.8 eV, vs. 2.0 eV for silicon, for example [20]), as well as the low Z-number of carbon, diamond is a highly radiation-hard material [21]. Diamond also has a wide, indirect bandgap of ~5.5 eV [22], which means that the collection distance for photogenerated carriers is relatively large [23]. For these reasons, diamond has already been used for alpha- and beta-voltaics [1,2], as well as for gamma/X-ray dosimeters and detectors [24,25]. Gamma dosimeters have been calibrated by some of the authors in a previous study up to 3600 Gy/h, showing no degradation [26]. Extensive research on diamond detectors has been undertaken at the University of Rome *Tor Vergata* [27–32]. Researchers there have tested their dosimeters under a wide range of radiation types, both with and without an applied bias. However, as the spatial measurement resolution of dosimeters is important, the *Tor Vergata* group has tended toward thinner sensitive volumes, down to 1 μm, and hence, lower gamma capture volumes. One such device produced ~23 nA under a synchrotron photon flux of 2×10^{11} γ.s^{-1} of 17.5 keV X-rays [28]. Their dosimeter has been successfully commercialized [25,33,34]. A lineage of diamond detector research has also be produced by the RD42 Collaboration [35], which is a collaboration intended to make use of, and serve, the Large Hadron Collider. Most notably, recent work from the

RD42 Collaboration has focused on the use of polycrystalline diamond [36,37], as has work from others in the past two decades [38–40]. In one case, a detector nearly 5 cm in diameter was created [38]. This is significant, as the difference in cost between electronic grade single-crystal and polycrystalline diamond is great. Also, large-area growth is far easier for polycrystalline diamond, with the upper limit for polycrystalline diamond being fixed at around 100 mm by the physical properties of a microwave growth plasma [41], whereas single crystals still tend to be found only in sizes of a few square millimeters. Development in this area for detectors may facilitate polycrystalline diamond gammavoltaic cells in the future, in a manner analogous to how polycrystalline solar cells offer a cheaper, even if less efficient, alternative to those that are monocrystalline [42].

A fundamental problem in the design of a diamond gamma-voltaic (DGV) is the correlation between gamma-ray capture cross-section, σ, and series resistance R_S. Gamma photons are very penetrating, and diamond is highly insulating [23,43]. In a pseudo-vertical Schottky diode structure, such as those used in other diamond radiovoltaics and the *Tor Vergata* detectors, increasing the sensitive volume in order to capture enough gamma photons to power external circuitry would lead to unacceptable device resistance, and hence, also prevent the device from generating enough power. Our novel solution to this problem, presented here, is to reduce the coupling of these two quantities via exploitation of the surface transfer doping effect. A bare, hydrogen-terminated diamond surface is conductive in air, with a resistance that varies with the coverage of terminating hydrogen, θ_H, or of the adsorbed layer of water vapor, which 'activates' the hydrogen sites via surface transfer-doping [44]. Hydrogen termination creates a low-resistivity two-dimensional hole gas (2DHG) [45,46]. The thickness, radiation hardness, and collection distance of the bulk are used to capture gamma rays and scatter showers of lower-energy electrons and photons toward the surface. Electrons that reach the surface are collected as current. The majority of the current is expected to flow around the surface rather than through the bulk. The problematic coupling between capture cross-section and series resistance is thus reduced. Fig. 1 shows the principles of this solution by comparison to the two other possible candidates.

In this paper, the effectiveness of terminating a device in this way is first tested using 160 kVp broadband X-ray irradiation. The terminated device is then tested under irradiation from a synchrotron beam, scanning over energies between approximately 50 - 150 keV. This range is of interest, as it covers several gamma emission energies, most prominently Am-241 [47] and a significant portion of the U-235* fission delayed-gamma spectrum [48]. This range is equally of interest because it is the range over which the
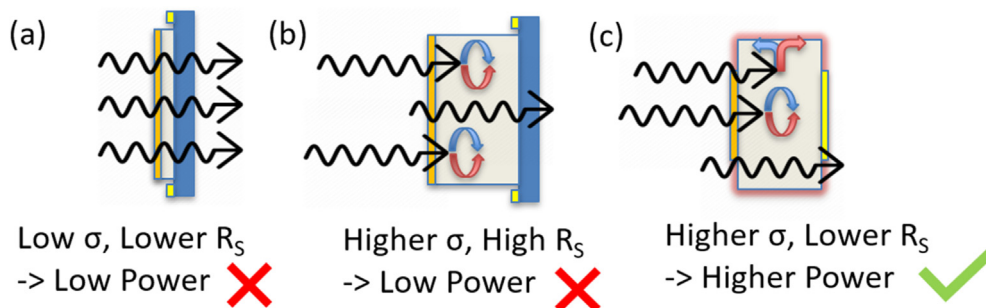
Fig. 1. Three possible designs for a DGV device, in which boron-doped diamond is represented as blue, intrinsic or low-doped diamond in beige, electrons and holes as blue and red arrows, respectively, ohmic or low-barrier contacts as yellow, high-barrier contacts as orange, and a hydrogen-terminated surface as a red glow. **(a)** Is a standard pseudo-vertical Schottky diode suitable for diamond alphavoltaics and betavoltaics, **(b)** is a similar device with a much thicker intrinsic region. **(c)** Is the design tested in this paper, in which the resistance of a thick capture volume is bypassed by allowing current to travel around the surface of the device. (For interpretation of the references to color in this figure legend, the reader is referred to the Web version of this article.)

photon interaction mechanism for diamond changes from the photoelectric effect (PE) to Compton scattering (CS) [49]. As such, it probes the impact of interaction mechanisms on device performance.

2. Materials and methods

2.1. Diamond gammavoltaic cell fabrication

In common with standard leakage-mode detectors, the core of the gammavoltaic device was an electronic-grade, single-crystal diamond, with dimensions $4.5 \times 4.5 \times 0.5$ mm, i.e. a surface area of 0.2 cm^2 (Element Six Ltd, Oxfordshire, UK). The crystal orientation was [100], and the nitrogen and boron impurities were specified to the order of parts per billion, equivalent to ~10^{14} cm^{-3} [43]. This ultra-pure, highly crystalline form was chosen in order to reduce the parameter space when trying to produce the device and to isolate the electrical effects of the surface.

The diamond was washed for 2 h in aqua regia at 65 °C, to remove any environmental contaminants and metal residues from prior use. 3.5×3.5 mm contacts were deposited, centrally located on opposing faces of the substrate. The contact layers were different metals—aluminum and 80/20 nichrome—to introduce barrier asymmetry, and hence, a built-in voltage. The contact layers were capped with gold under the same vacuum to avoid oxidation. Metals were deposited via physical vapor deposition using resistive thermal evaporation, through shadow masks, in an Edwards 306 Thermal Evaporator. The base pressure was ~4.5 µTorr (0.6 mPa). The substrate was heated to 250 °C during deposition and for 1 h beforehand to remove adsorbed water, nitrogen, and adventitious carbon. After deposition, the device was not annealed.

As a final cleaning and oxygen terminating step for the exposed surfaces of the device, a modified sputter coater (the 'Terminator') was used, wherein a DC oxygen plasma was struck at ~3 kV and 1 Torr (133.3 Pa) for 30 s. For hydrogen termination, the Terminator chamber was then re-pumped and used to strike a hydrogen plasma, also at ~3 kV and 1 Torr (133.3 Pa) for 30 s. This created a surface hydrogen monolayer coverage $\theta_H \approx 0.3$, as measured by X-ray photoemission spectroscopy (see supporting information §S1). Sample size restrictions limited spatial information on coverage; it was assumed that this partial coverage was homogenous. The standard method of producing a hydrogen termination on a given diamond substrate is to treat a substrate to a microwave-enhanced hydrogen plasma, which has the added benefit of happening automatically during growth for those that grow their own substrates [50,51]. This was not suitable for this application due to the need for the contacts to be deposited prior to termination; the conditions of a microwave plasma are too harsh for unannealed metal contacts. The same device was used for both tests to isolate, as far as possible, the effect of the surface termination.

For electrical testing, the device was mounted onto an SMA head with silver conductive epoxy paint, as shown in Fig. 2. The assembly was left to dry, then baked in an oven at 120 °C for 10 min to cure the silver epoxy. We do not believe that the curing process will have had any great effect on the surface, as it has been shown that the surface conductivity of hydrogen-terminated diamond remains relatively stable to 120 °C even *in vacuo* [44]. However, the device was left undisturbed for approximately one day prior to any testing to ensure the re-adsorption of any lost surface water.

2.2. I−V testing

2.2.1. Using a broadband X-ray source

A Zeiss Xradia Versa 520 X-ray Tomography microscope (XRT) was used to test whether hydrogen termination is indeed necessary
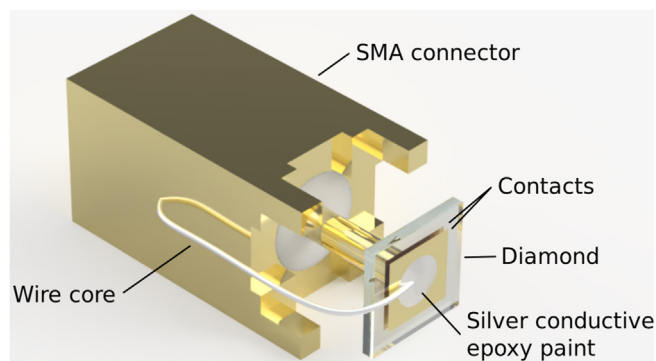
Fig. 2. A rendering of the test mounting used for the DGV cell.

for creating a gammavoltaic effect by illuminating the same device both before and after the introduction of any terminating hydrogen. For these tests, the X-ray source, which used a tungsten target and was unfiltered except by air, was set to 160 kV accelerating voltage and 9 W power. The characteristic emission lines of tungsten in this range are $K\alpha_2 \approx 58.0$ keV and $K\alpha_1 \approx 59.3$ keV [52]. The dose rate was unknown.

$I−V$ curves were taken in air, with the bias applied and the current measured with a Keithley 6517A multimeter. The bias was increased in increments of 0.05 V, between 0 and 0.55 V for the device before partial hydrogen termination, and between 0 and 1 V for the device after partial hydrogen termination, and 10 measurements were taken per increment. A 0.1 s dwell time was employed at the start of each increment to allow any capacitative effects to settle.

2.2.2. At the Diamond Light Source synchrotron

Use of the I12 beamline [53] at the DLS synchrotron allowed the DGV to be driven with a high-brightness beam of near-monochromatic X-rays, between 53.6 and 148.4 keV, of calculable flux. Measurements were performed with the beamline's Laue monochromator crystals unbent to provide the narrowest possible photon energy bandwidth. After this, the energy was returned to a middle value, 81.1 keV, to seek evidence of damage or hysteresis. $I−V$ curves were taken approximately 30 min apart. The beamline has controllable flux. However, this is achieved through aperture size. Because it was desirable to keep the irradiated device surface area constant, the $I−V$ curves were scaled to the flux at 53.6 keV: the current measured at each applied bias was multiplied by the ratio of the flux during that run to the flux during the 53.6 keV run. Scaling $I−V$ curves in this way is fully valid only if the change in series resistance R_S, due to flux changes, can be taken as zero over the range of fluxes employed and the open-circuit voltage (V_{OC}) remains constant. Experiments with the XRT showed that the resistance criterion is met at relatively low fluxes, far lower than those attained by the synchrotron. The V_{OC} criterion was tested as part of the experiment. Fig. S3 in the supporting information (§S2) shows the synchrotron fluxes used in the experiment. The flux had a maximum of 2×10^{11} γ.s^{-1} at 53.6 keV and dropped to 8×10^9 γ.s^{-1} by 148.4 keV. The $I−V$ curves should thus be read as normalized to 2×10^{11} γ.s^{-1} incident flux. Resistance extraction was performed using the current offset method [54], detailed in full in the supporting information (§S3). $I−V$ curves were taken in the air. Before exposing the cell to each incident wavelength, the energy of the beam was measured using X-ray diffraction from a NIST Standard Reference Material® 674b CeO_2 powder sample. The $I−V$ curves were taken using the same measurement parameters as listed in §2.2.1, between 0 and 1 V.

The DLS experiment occurred 31 days after the XRT experiment, and the device was not altered or modified within that time.

3. Results

3.1. Necessity of hydrogen termination for DGV function

$I–V$ data, taken from the device, driven by the XRT, with no hydrogen coverage ($\theta_H = 0.0$) and after partial hydrogen coverage ($\theta_H \approx 0.3$), are shown in Fig. 3. The device produced only a small gammavoltaic effect with no hydrogen coverage, generating currents of the order of 10 pA, in line with what would be expected from a monolithic insulating crystal. The fill factor FF = P_{max}/P_{theo} where $P_{theo} = I_{SC} \times V_{OC}$, a figure of merit for photovoltaic cells, was not considered sensibly calculable due to the form of the $P–V$ curve. When the partial hydrogen termination was applied, the device showed a clear gammavoltaic effect, with a short-circuit current $I_{SC} = 0.4$ μA, four orders of magnitude greater than the previous experiment, a $V_{OC} = 0.8$ V and an FF = 0.43 ± 0.01.

3.2. DGV driven by synchrotron radiation for key parameter extraction over Compton crossover region

Fig. 4 shows the I–V and associated P–V characteristics of the DGV with $\theta_H \approx 0.3$, under irradiation from energies between approximately 50 - 150 keV at the DLS synchrotron. $\Delta I(\Delta V)$ points are also marked on the figure, where $\Delta I = I_{SC} - \delta I$, $\delta I = 800$ nA and ΔV is the applied bias at which ΔI was measured. These points were used for resistance extraction and were found to be well-fit by a phenomenological exponential function,

$$\Delta I = Ae^{\frac{-V}{B}} + C, \tag{1}$$

for which $A = 24 \pm 1$ μA, $B = 200 \pm 7$ mV, and $C = -400 \pm 60$ nA are fitting constants. The inverse of the derivative of this function was used to determine the changing series resistance of the device with incident photon energy.

The device parameters for the device are shown in Fig. 5. The adjusted I_{SC} increases gradually with photon energy, up to a maximum of ~10 μA. There is some hysteresis in the V_{OC}, but the value remains roughly constant around 0.82 V. The constancy in the V_{OC} leads the P_{max} to essentially follow the I_{SC}. The measurements taken to look for evidence of degradation, after the main run from 53.6 to 148.4 keV, at 81.1 keV, show no marked difference to what was seen during the run. The R_S decreases over the range. It is displayed alongside a subfigure derived from literature data [49], which is the percentage of photon interactions taking place via Compton scattering (as opposed to the photoelectric effect) over this energy range. There is a very good inverse agreement between these two quantities.

4. Discussion

The test of the device with full oxygen termination (i.e. before partial hydrogen termination) and after partial hydrogen termination ($\theta_H \approx 0.3$) showed conclusively that the partial hydrogen termination was necessary for gammavoltaic behavior. This validates the design principle put forward in this paper, suggesting that creating a conductive surface does indeed capture scattered secondary particles from photons interacting with the bulk. As the hydrogen termination is a single atomic layer, the capture cross-section would be too low for this output to come solely from photons interacting at the surface. However, it remains unknown whether the entire bulk takes part in the mechanism or whether a shallower subsurface region is responsible. The fill factor of 0.43 ± 0.01 was quite low—contemporary solar cells can reach
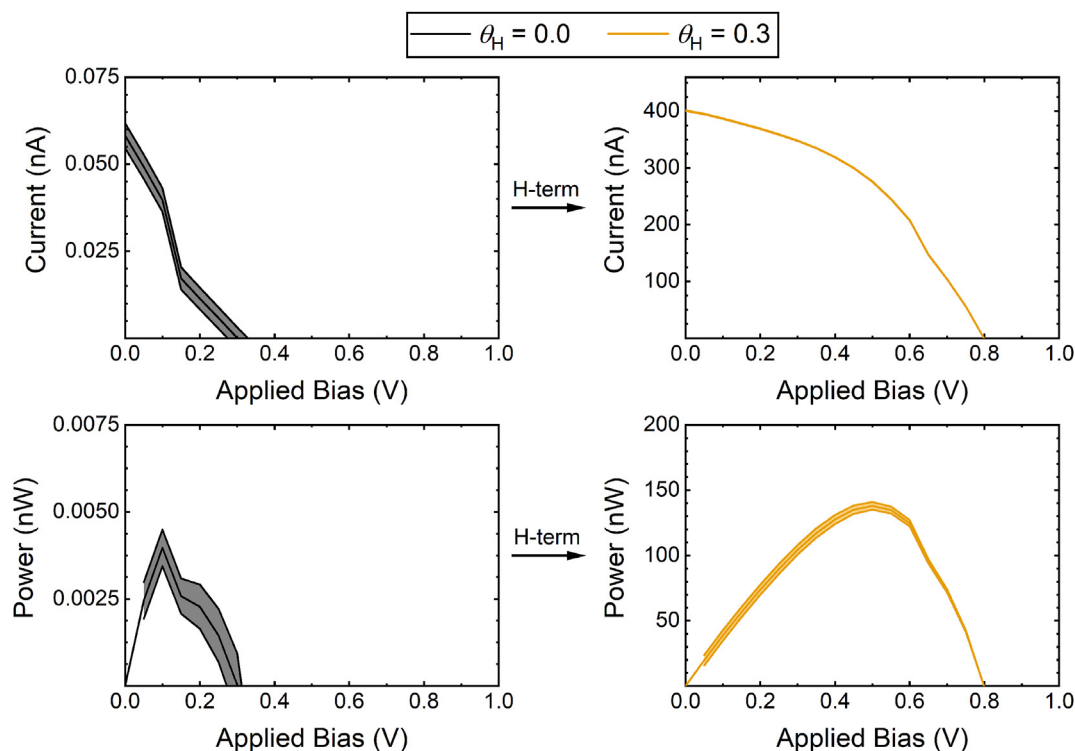
Fig. 3. I–V curves, taken with the device and the related P–V curves, first with no hydrogen coverage, and then with $\theta_H \approx 0.3$ as estimated with XPS. The devices were driven with broadband X-rays from the XRT. Uncertainty in the hydrogen-terminated I–V case was <10 nA.
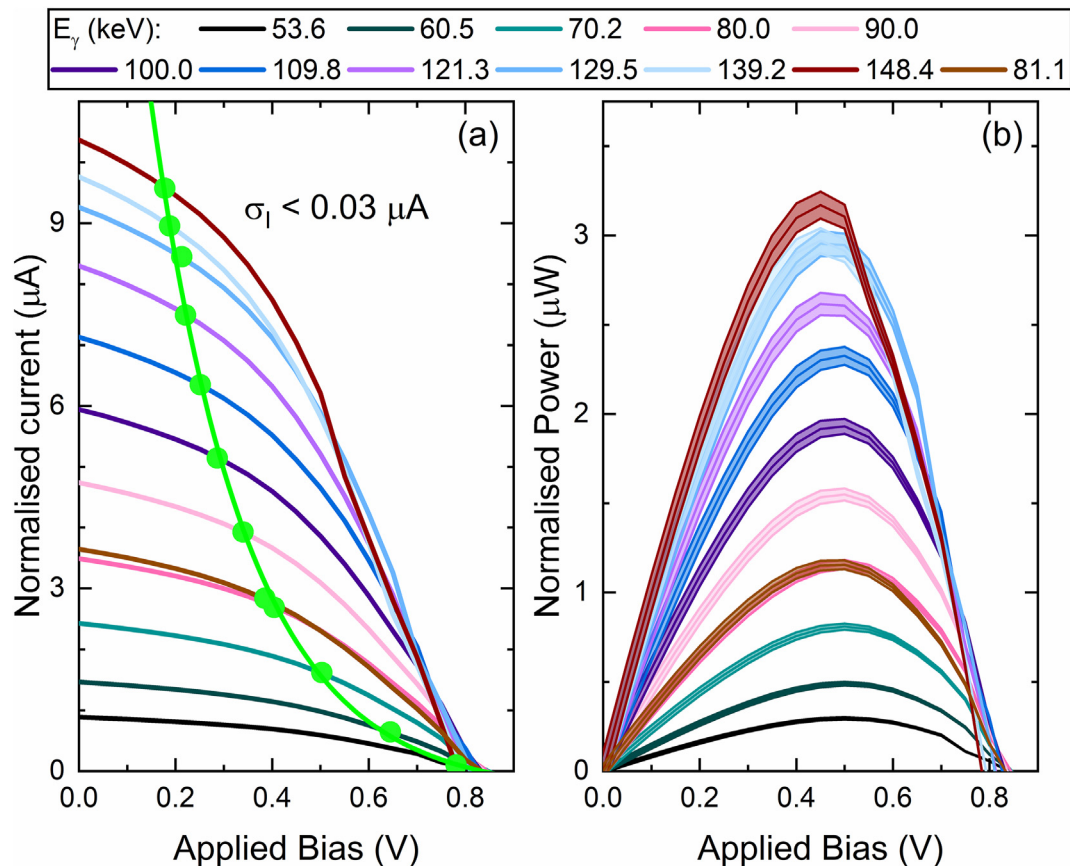
Fig. 4. (a) I−V and **(b)** P−V data taken under irradiation from various photon energies. The responses have been scaled in flux relative to the flux of 53.6 keV photons (see §2.2.1). Error bands correspond to instrument accuracy, which had a larger error than the statistical error. The green circles are ΔI (ΔV) points for resistance extraction, where $\Delta I = I_{SC} - \delta I$ the constant offset δI = 800 nA and ΔV is the read-off bias at which this value occurs on the trace. The green line is a phenomenological exponential decay fit described by Equation (1), with $R^2 > 0.996$. The 81.1 keV trace was measured after the run from 53.6 to 148.4 keV. (For interpretation of the references to color in this figure legend, the reader is referred to the Web version of this article.)

FF > 0.8 [55,56]. This is likely due to both shunt and series device resistances, visible in the gradual slopes of the trace, in contrast to the ideal step shape. Both quantities are expected to be strongly determined by the hydrogen coverage. The hydrogen coverage, 0.3, was relatively low and is not optimized. However, future work involving temperature control in the Terminator should allow more control over hydrogen coverage, and hence, the exploration of the parameter space. As the 2DHG resistivity can change by orders of magnitude with different adsorbate coverages [44] it is likely that this parameter will significantly affect device performance and act as an avenue for improvement. It is not certain that as high a coverage as possible would be optimal; a coverage too high may short the device or reduce the ability of the surface to collect charge carriers. It is expected, at present, that a medium-low hydrogen coverage may be optimal for this type of device, with the surface hydrogen acting similarly to a dopant in a conventional semiconductor junction; high enough in concentration to allow current to flow, but low enough that the region may be depleted by the high-barrier contact, and hence, collect the charge. It may be that this view is mistaken and that, in fact, as high a hydrogen coverage as possible is desirable. In this case, a stable and reproducible bulk counterpart to the surface termination would be graphite pillar electrodes. These are increasingly prevalent in diamond detectors [36,57−62] but also have the distinction of having worked well in an energy device: the diamond photon-enhanced thermionic energy converter of Girolami et al. [63].

While no obvious damage occurred to the device during the DLS experiment itself, it failed to operate in later experiments. It is unlikely that this damage was within the bulk crystal or contacts, as the performance was later entirely regenerated by reterminating and remounting. Possible sources of degradation are catastrophic resistance increase caused by desorption of surface hydrogen [44,64], simple manual handling issues, and/or structural damage to the silver epoxy adhesive by X-rays. These latter two issues would be due to the prototypical nature of the test mounting. On hydrogen desorption: researchers have cautioned against using hydrogen-terminated diamond surfaces as the basis of transistors in the past due to stability concerns [44]. However, more recently, there has been great progress in stabilizing the surface for applications in high temperatures [65]. Using the passive electrically depleting effect of a deposited HfO_2 layer and Ti/Au contacts, one group has even created a normally off MOSFET based on hydrogen-terminated diamond [66], suggesting that the use of an encapsulating layer has distinct potential both for stabilizing and enhancing the DGV. Should it become apparent in future that surface desorption is a major route of device degradation, these established methods will be the first avenue of enquiry for solutions. It is, of course, not logical to use diamond for its bulk radiation hardness if the surface termination is overly sensitive.

That the V_{OC} does not follow a theoretical relationship is to be expected, as the flux scaling process erroneously treats the V_{OC}. The fact that V_{OC} shrinks with photon energy here is not a physical truth but is related to the fact that original fluxes at higher energies
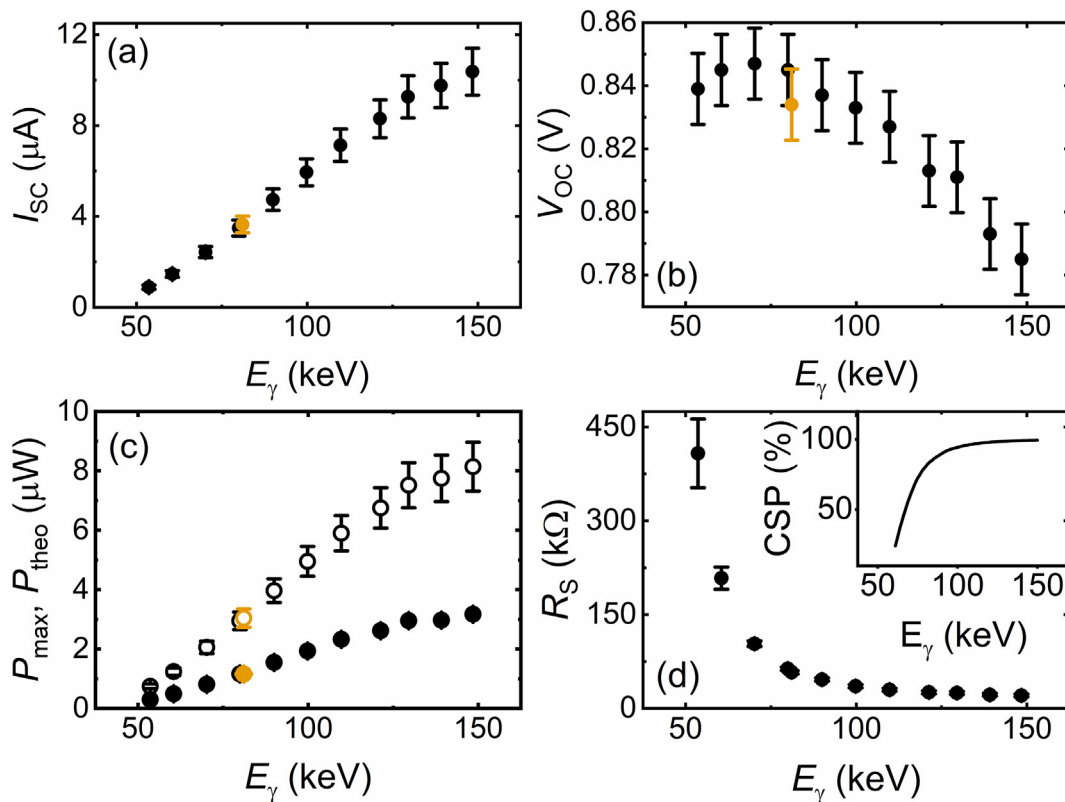
Fig. 5. Parameters extracted from Fig. 4. (a) Is the DGV short-circuit current I_{SC}. **(b)** Is the open-circuit voltage V_{OC}. The V_{OC} is not legitimately treated by this scaling method, hence the gradual decrease with energy; this is due to the decreasing flux with energy in the raw data. **(c)** Shows the maximum power P_{max} (**closed circles**) and theoretical maximum power $P_{theo} = I_{SC} \times V_{OC}$ (**open circles**). **(d)** Shows series resistance R_S of the device. Also shown, for comparison, are calculated cross-section data for the proportion of interactions that are Compton scattering events [49] **(inset)**. The measurement taken after the others, at 81.1 eV, is shown in orange for clarity in subfigures **(a–c)**, but not in **(d)** as time information is lost in the resistance extraction process. (For interpretation of the references to color in this figure legend, the reader is referred to the Web version of this article.)

were lower. However, the range in V_{OC} is low enough that the extraction of the other parameters could proceed.

There is a very good qualitative agreement between the drop in series resistance and the proportion of photon interactions that proceed via CS. In this transitory range, a photon may interact via either PE or CS. However, it will do so with differing probabilities related to its energy. Both PE and CS events will ionize multiple lattice sites in the region around the initial impact. PE interactions generate a single high-energy electron, which then goes on to scatter inside the lattice and eventually thermalize. CS interactions similarly generate a high-energy electron but also a more penetrating high-energy photon [67]. This photon may then cause a PE or CS interaction of its own. A photon may traverse the entirety of the crystal within 36 ps, whereas the specified average carrier lifetime is ~2 μs for crystals of this purity [43]. The initial impact and the impact of a secondary photon, therefore, happen simultaneously from the perspective of charge carrier creation. The ionization region of a CS interaction in a given moment is, therefore, greater, and CS-dominated operation will exhibit lower series resistance, as regions have a greater chance of touching and leading to conductive paths. This effect may be expected just as much in a fully oxygen-terminated device as in a partially hydrogen-terminated device, so the scattering mechanism alone cannot lead to a significant gammavoltaic effect. We suggest that the partial hydrogen termination acts to lower the flux and energy thresholds at which conductive paths caused by illumination may occur by providing a network of nodes, which may be connected by the paths as they form. This provides further motivation to optimize the surface coverage. The comparison must also be drawn to work

by Conte et al. [68], in which MESFETs based on the hydrogen-terminated diamond were triggered by UV pulses, which turned the devices on via photogenerated holes. By this comparison, our DGV can be considered a 'Compton-enhanced' device, much as these MESFETs were 'UV-triggered'.

The changing series resistance means it is more challenging than might be expected to simulate the DGV using standard high energy physics simulation software such as GEANT4 [69] or MCNP [70], as has been done in the previous radiovoltaic [2,4,71,72] and dosimeter research [31,73,74]. The energy deposited into the device, as simulated by such software, is not straightforwardly related to the power produced by some constant efficiency factor. We are currently working to develop a model that describes the way in which high-energy physics and surface electrical physics combine in our device in a manner similar to that which has been reported by authors who combined GEANT4 and TCAD simulations for simulating diamond detectors [75].

The single DGV cell presented here produced a voltage on par with other photovoltaics, which tends to produce open-circuit voltages in the range of 0.5–1.2 V per cell. There is no established method of reporting gammavoltaic performance, not least because gamma rays can have such a wide range of energies, and as such, there is no equivalent to the AM1.5 solar spectrum used for other photovoltaics. Previous research is still, for the most part, too variable for direct comparison. However, application power requirements can be used as a benchmark. Micropower harvesting chips require similar values, with the Advanced Linear Devices EH300 [76], for example, requiring 200 nA at 4 V. As such, the cell performance is sufficiently promising that deployments of

multi-cell devices in Co-60 and Cs-137 fields is now ongoing, so that the device may be measured against these real-world requirements, and benchmarked against other gammavoltaic devices that have used these common waste isotopes as sources. Based on this work, we believe that a multi-cell DGV of this type will be able to satisfy the energy requirements of low-power sensor pods operating remotely and wirelessly in nuclear waste stores and repositories.

5. Conclusions

We have shown that the DGV presented here, made according to our novel design principle but not optimized, generates sufficient power to be a promising candidate for further development. By allowing current to be captured and conducted around the surface while generating, capturing, and scattering high-energy photons in the radiation hard, insulating bulk, we have partially decoupled the collection volume cross-section and the series resistance. There remain limitations, crucially, the stability of the hydrogen termination. This, along with a general optimization of the surface in terms of hydrogen coverage, will be the subject of future work. A partial hydrogen coverage was proved to be necessary to gammavoltaic behavior in the device, validating the underlying design principles. The voltage generated by a single cell was ~0.8 V, with example power outputs being 295 nW at 50 keV and 3.17 μW at 150 keV, for 2×10^{11} $\gamma.s^{-1}$ incident flux. In the long term, another limitation is the cost of the substrates necessary to make a DGV of this type and the attainable surface area of a single cell when using a single-crystal diamond. Future work may explore the effectiveness of cheaper, larger polycrystalline devices. The series resistance of the device was found to decrease with increasing energy, in good agreement with the increasing prevalence of Compton scattering. It is hypothesized that this is caused by the increased ionization radius around a Compton scattering site, facilitated by partial hydrogen termination providing nodes for ionized corridors to connect to. Work is now ongoing to test multi-cell devices in a range of Co-60 and Cs-137 dose rates, with preliminary results suggesting useful power outputs may be attained in the near-term.

Data statement

Both the raw and processed data required to reproduce these findings are available to download from https://doi.org/10.17632/z2njptskdj.1, and are also provided alongside the supplementary information.

CRediT authorship contribution statement

G.R. Mackenzie: Conceptualization, Methodology, Software, Formal analysis, Investigation, Data curation, Writing − original draft, Visualization, Project administration. **S. Kaluvan:** Conceptualization, Validation, Project administration. **P.G. Martin:** Investigation, Writing − review & editing, Project administration. **C. Hutson:** Conceptualization, Methodology, Software, Investigation, Resources, Writing − review & editing, Supervision, Project administration. **T. Connolley:** Methodology, Validation, Investigation, Resources, Writing − review & editing, Supervision, Project administration. **M. Cattelan:** Methodology, Validation, Formal analysis, Investigation, Resources, Writing − review & editing, Supervision, Project administration. **H. Dominguez-Andrade:** Conceptualization, Methodology, Writing − review & editing, Supervision. **T.L. Martin:** Writing − review & editing, Supervision. **N.A. Fox:** Conceptualization, Supervision, Project administration, Funding acquisition. **T.B. Scott:** Conceptualization,

Writing − review & editing, Supervision, Project administration, Funding acquisition.

Declaration of competing interest

The authors declare that they have no known competing financial interests or personal relationships that could have appeared to influence the work reported in this paper.

Appendix A. Supplementary data

Supplementary data to this article can be found online at https://doi.org/10.1016/j.mtener.2021.100688.

References

[1] B. Liu, B. Dai, K. Liu, L. Yang, J. Zhao, G. Shu, Z. Lv, G. Gao, K. Yao, M. Bi, J. Xue, W. Wang, V. Ralchenko, J. Han, J. Zhu, Alpha-voltaic battery on diamond Schottky barrier diode, Diam. Relat. Mater. 87 (2018) 35−42, https://doi.org/10.1016/j.diamond.2018.05.008.

[2] V. Bormashov, S. Troschiev, A. Volkov, S. Tarelkin, E. Korostylev, A. Golovanov, M. Kuznetsov, D. Teteruk, N. Kornilov, S. Terentiev, S. Buga, V. Blank, Development of nuclear microbattery prototype based on Schottky barrier diamond diodes, Phys. Status Solidi Appl. Mater. Sci. 212 (2015) 2539−2547, https://doi.org/10.1002/pssa.201532214.

[3] C. Haiyang, Y. Jianhua, L. Darang, Electrode pattern design for GaAs betavoltaic batteries, J. Semiconduct. 32 (2011), 084006, https://doi.org/10.1088/1674-4926/32/8/084006.

[4] J. Russo, M. Litz, W. Ray, S. Bayne, G.M. Rosen, H. Cho, J. Yu, D.I. Bigio, C. Thomas, T.R. Alam, Demonstration of a tritiated nitroxide nuclear battery, Appl. Radiat. Isot. 144 (2019) 93−103, https://doi.org/10.1016/j.apradiso.2018.10.012.

[5] S.I. Maximenko, J.E. Moore, C.A. Affouda, P.P. Jenkins, Optimal semiconductors for 3H and 63Ni betavoltaics, Sci. Rep. 9 (2019) 1−8, https://doi.org/10.1038/s41598-019-47371-6.

[6] C.B. Honsberg, W.A. Doolittle, M. Allen, C. Wang, GaN betavoltaic energy converters, in: IEEE Photovoltaics Spec. Conf., 2005, pp. 102−105, https://doi.org/10.1109/PVSC.2005.1488079.

[7] R.G. Helmer, C.W. Reich, An excited state of Th 229 at 3.5 eV, Phys. Rev. C 49 (1994) 1845−1858, https://doi.org/10.1103/PhysRevC.49.1845.

[8] American Society for Testing and Materials, Reference Air Mass 1.5 Spectra G-173, (n.d.). https://www.nrel.gov/grid/solar-resource/spectra-am1.5.html. (Accessed 17 September 2020).

[9] M.J. Berger, J.H. Hubbell, S.M. Seltzer, J. Chang, J.S. Coursey, R. Sukumar, D.S. Zucker, K. Olsen, NIST XCOM: Photon Cross Sections Database, (n.d.). https://doi.org/10.18434/T48G6X.

[10] K. Scharf, Photovoltaic effect produced in silicon solar cells by X-and gamma rays, J. Res. Natl. Bur. Stand. A. Phys. Chem. 64 (1960) 297−307, https://doi.org/10.6028/jres.064A.029.

[11] K. Hashizume, H. Kimura, T. Otsuka, T. Tanabe, T. Okai, Direct energy conversion from gamma ray to electricity using silicon semiconductor cells, MRS Proc. 1264 (2010), https://doi.org/10.1557/PROC-1264-BB05-01. 1264-BB05-01.

[12] N. Horiuchi, K. Taniguchi, M. Kamiki, T. Kondo, M. Aritomi, The characteristics of solar cells exposed to γ-radiation, Nucl. Instruments Methods Phys. Res. Sect. A Accel. Spectrometers, Detect. Assoc. Equip. 385 (1997) 183−188, https://doi.org/10.1016/S0168-9002(96)01046-7.

[13] J.R. White, D. Kinsman, T.M. Regan, L.M. Bobek, Novel Nuclear Powered Photocatalytic Energy Conversion, 2005. https://www.osti.gov/servlets/purl/850408. (Accessed 2 June 2020).

[14] B. Náfrádi, G. Náfrádi, F. László, L. Lászlóforró, E. Horváth, Methylammonium lead iodide for efficient X-ray energy conversion, J. Phys. Chem. C 119 (2015) 25204−25208, https://doi.org/10.1021/acs.jpcc.5b07876.

[15] G. Náfrádi, E. Horváth, M. Kollár, A. Horváth, P. Andričević, A. Sienkiewicz, L. Forró, B. Náfrádi, Radiation detection and energy conversion in nuclear reactor environments by hybrid photovoltaic perovskites, Energy Convers. Manag. 205 (2020) 112423, https://doi.org/10.1016/j.enconman.2019.112423.

[16] Q. Dong, Y. Fang, Y. Shao, P. Mulligan, J. Qiu, L. Cao, J. Huang, Electron-hole diffusion lengths > 175 μm in solution-grown CH3NH3PbI3 single crystals, Science (80-.) 347 (2015) 967−970, https://doi.org/10.1126/science.aaa5760.

[17] S. Yakunin, D.N. Dirin, Y. Shynkarenko, V. Morad, I. Cherniukh, O. Nazarenko, D. Kreil, T. Nauser, M.V. Kovalenko, Detection of gamma photons using solution-grown single crystals of hybrid lead halide perovskites, Nat. Photon. 10 (2016) 585−589, https://doi.org/10.1038/nphoton.2016.139.

[18] J.K. Liakos, Gamma-ray-driven photovoltaic cells via a scintillator interface, J. Nucl. Sci. Technol. 48 (2011) 1428−1436, https://doi.org/10.1080/18811248.2011.9711836.

[19] J.K. Liakos, Thorium-229m1/m2-powered heterojunction GRPVCs: an interface between nuclear and semiconductor physics, Semicond, Sci. Technol. 24 (2009), 065001, https://doi.org/10.1088/0268-1242/24/6/065001.

[20] A.V. Lysenko, Interatomic bond energy and analytical scale of hardness, J. Superhard Mater. 39 (2017) 25−33, https://doi.org/10.3103/S1063457617010038.

[21] T. Behnke, M. Doucet, N. Ghodbane, A. Imhof, C. Martínez, W. Zeuner, Electromagnetic radiation hardness of diamond detectors, Nucl. Instruments Methods Phys. Res. A Accel. Spectrometers, Detect. Assoc. Equip. 489 (2002) 230−240, https://doi.org/10.1016/S0168-9002(02)00572-7.

[22] G. Calzaferri, R. Rytz, The band structure of diamond, J. Phys. Chem. 100 (1996) 11122−11124, https://doi.org/10.1021/jp960840t.

[23] R.S. Balmer, J.R. Brandon, S.L. Clewes, H.K. Dhillon, J.M. Dodson, I. Friel, P.N. Inglis, T.D. Madgwick, M.L. Markham, T.P. Mollart, N. Perkins, G.A. Scarsbrook, D.J. Twitchen, A.J. Whitehead, J.J. Wilman, S.M. Woollard, Chemical vapour deposition synthetic diamond: materials, technology and applications, J. Phys. Condens. Matter 21 (2009) 364221, https://doi.org/10.1088/0953-8984/21/36/364221.

[24] E.A. Burgemeister, Dosimetry with a diamond operating as a resistor, Phys. Med. Biol. 26 (1981) 269−275, https://doi.org/10.1088/0031-9155/26/2/006.

[25] B. Caiffi, I. Coffey, M. Pillon, M. Osipenko, G. Prestopino, M. Ripani, M. Taiuti, C. Verona, G. Verona-Rinati, Analysis of the response of CVD diamond detectors for UV and sX-ray plasma diagnostics installed at JET, in: Phys. Procedia, Elsevier B.V., 2015, pp. 79−83, https://doi.org/10.1016/j.phpro.2015.02.014.

[26] C. Hutson, L. Payne, T. Scott, A. Jenkins, Deployment of diamond-based radiation detector for very high dose rate measurements, in: 43rd Annu. Waste Manag. Conf. Educ. Oppor. Waste Manag., Waste Management Symposia, Inc, Phoenix, Arizona, USA, 2017.

[27] S. Almaviva, M. Marinelli, E. Milani, A. Tucciarone, G. Verona-Rinati, R. Consorti, A. Petrucci, F. De Notaristefani, I. Ciancaglioni, Synthetic single crystal diamond diodes for radiotherapy dosimetry, Methods Phys. Res. A 594 (2008) 273−277, https://doi.org/10.1016/j.nima.2008.06.028.

[28] S. Almaviva, M. Marinelli, E. Milani, G. Prestopino, A. Tucciarone, C. Verona, G. Verona-Rinati, M. Angelone, M. Pillon, I. Dolbnya, K. Sawhney, N. Tartoni, Chemical vapor deposition diamond based multilayered radiation detector: physical analysis of detection properties, J. Appl. Phys. 107 (2010), 014511, https://doi.org/10.1063/1.3275501.

[29] M. Marinelli, E. Milani, G. Prestopino, C. Verona, G. Verona-Rinati, M. Angelone, M. Pillon, V. Kachkanov, N. Tartoni, M. Benetti, D. Cannatà, F. Di Pietrantonio, F. Di Pietrantonio, Synchrotron Radiation X-ray beam monitor made by thin-film CVD single-crystal diamond, J. Synchrotron Radiat. 19 (2012) 1015−1020, https://doi.org/10.1107/S0909049512038186.

[30] G. Prestopino, M. Marinelli, E. Milani, C. Verona, G. Verona-Rinati, Transient lateral photovoltaic effect in synthetic single crystal diamond, Appl. Phys. Lett. 111 (2017) 143504, https://doi.org/10.1063/1.4994120.

[31] C. Verona, G. Magrin, P. Solevi, V. Grilj, M. Jakšić, R. Mayer, M. Marinelli, G. Verona-Rinati, Spectroscopic properties and radiation damage investigation of a diamond based Schottky diode for ion-beam therapy microdosimetry, J. Appl. Phys. 118 (2015) 184503, https://doi.org/10.1063/1.4935525.

[32] S. Rollet, M. Angelone, G. Magrin, M. Marinelli, E. Milani, M. Pillon, G. Prestopino, C. Verona, G. Verona-Rinati, A novel microdosimeter based upon artificial single crystal diamond, IEEE Trans. Nucl. Sci. 59 (2012) 2409−2411, https://doi.org/10.1109/TNS.2012.2209677.

[33] J. Damodar, D. Odgers, D. Pope, R. Hill, A study on the suitability of the PTW microDiamond detector for kilovoltage X-ray beam dosimetry, Appl. Radiat. Isot. 135 (2018) 104−109, https://doi.org/10.1016/j.apradiso.2018.01.025.

[34] A. Chalkley, G. Heyes, Evaluation of a synthetic single-crystal diamond detector for relative dosimetry measurements on a CyberKnife™, Br. J. Radiol. 87 (2014), https://doi.org/10.1259/bjr.20130768.

[35] CVD Diamond Radiation Detector Development: RD42 Collaboration, (n.d.). http://rd42.web.cern.ch/rd42/. (Accessed 25 January 2021).

[36] M. Reichmann, A. Alexopoulos, M. Artuso, F. Bachmair, L. Bäni, M. Bartosik, J. Beacham, H. Beck, V. Bellini, V. Belyaev, B. Bentele, A. Bes, J.M. Brom, M. Bruzzi, G. Chiodini, D. Chren, V. Cindro, G. Claus, J. Collot, J. Cumalat, A. Dabrowski, R. D'Alessandro, D. Dauvergne, W. de Boer, S. Dick, C. Dorfer, M. Dünser, G. Eigen, V. Eremin, G.T. Forcolin, J. Forneris, L. Gallin-Martel, M.L. Gallin-Martel, K.K. Gan, C. Gastal, C. Giroletti, M. Goffe, J. Goldstein, A. Golubev, A. Gorišek, E. Grigoriev, J. Grosse-Knetter, A. Grummer, B. Gui, M. Guthoff, B. Hiti, D. Hits, M. Hoeferkamp, T. Hofmann, J. Hosselet, J.Y. Hostachy, F. Hügging, C. Hutton, J. Janssen, H. Kagan, K. Kanxheri, G. Kasieczka, R. Kass, M. Kis, G. Kramberger, S. Kuleshov, A. Lacoste, S. Lagomarsino, A. Lo Giudice, I.L. Paz, E. Lukosi, C. Maazouzi, I. Mandic, A. Marino, C. Mathieu, M. Menichelli, M. Mikuž, A. Morozzi, J. Moss,

R. Mountain, A. Oh, P. Olivero, D. Passeri, H. Pernegger, R. Perrino, M. Piccini, F. Picollo, M. Pomorski, R. Potenza, A. Quadt, F. Rarbi, A. Re, S. Roe, D.A.S. Becerra, M. Scaringella, C.J. Schmidt, E. Schioppa, S. Schnetzer, S. Sciortino, A. Scorzoni, S. Seidel, L. Servoli, D.S. Smith, B. Sopko, V. Sopko, S. Spagnolo, S. Spanier, K. Stenson, R. Stone, B. Stugo, C. Sutera, B. Tannenwald, M. Traeger, W. Trischuk, D. Tromson, M. Truccato, C. Tuve, J. Velthuis, N. Venturi, S. Wagner, R. Wallny, J.C. Wang, J. Weingarten, C. Weiss, N. Wermes, M. Yamouni, M. Zalieckas, M. Zavrtanik, P.S. Salter, M. Chmeissani, S. Grinstein, D.V. Furelos, New test beam results of 3D and pad detectors constructed with poly-crystalline CVD diamond, Nucl. Instruments Methods Phys. Res. Sect. A Accel. Spectrometers, Detect. Assoc. Equip. 958 (2020) 162675, https://doi.org/10.1016/j.nima.2019.162675.

[37] J. Janssen, Test beam results of ATLAS DBM pCVD diamond detectors using a novel threshold tuning method, J. Instrum. 12 (2017), C03072, https://doi.org/10.1088/1748-0221/12/03/C03072.

[38] L. Liu, X. Ouyang, J. Zhang, X. Zhang, Y. Zhong, Polycrystalline CVD diamond detector: fast response and high sensitivity with large area Charge-carrier properties in synthetic single-crystal diamond measured with the transient-current technique Polycrystalline CVD diamond detector: fast response and hi, AIP Adv. 4 (2014), https://doi.org/10.1063/1.3275501.

[39] G. Conte, M. Girolami, S. Salvatori, V. Ralchenko, X-ray diamond detectors with energy resolution, Appl. Phys. Lett. 91 (2007) 183515, https://doi.org/10.1063/1.2805221.

[40] D. Tromson, A. Brambilla, F. Foulon, C. Mer, B. Guizard, R. Barrett, P. Bergonzo, Geometrical non-uniformities in the sensitivity of polycrystalline diamond radiation detectors, Diam. Relat. Mater. 9 (2000) 1850−1855, https://doi.org/10.1016/S0925-9635(00)00334-4.

[41] A. Matsushita, N. Fujimori, Y. Tsuchida, N. Ohtani, D. Dojima, K. Koide, T. Kaneko, S. Shikata, Evaluation of diamond mosaic wafer crystallinity by electron backscatter diffraction, Diam. Relat. Mater. 101 (2020) 107558, https://doi.org/10.1016/j.diamond.2019.107558.

[42] L. Rubin, Crystalline silicon solar cells and modules, in: L.M. Fraas, L.D. Partain (Eds.), Sol. Cells Their Appl., second ed., John While & Sons, 2010, p. 115.

[43] The Element Six CVD Diamond Handbook, (n.d.). https://e6cvd.com/media/wysiwyg/pdf/E6_CVD_Diamond_Handbook_A5_v10X.pdf. (Accessed 16 September 2020).

[44] O.A. Williams, R.B. Jackman, Surface conductivity on hydrogen terminated diamond, Semicond. Sci. Technol. 18 (2003) S34−S40, https://doi.org/10.1088/0268-1242/18/3/305.

[45] F. Maier, M. Riedel, J. Ristein, L. Ley, Origin of surface conductivity in diamond, Phys. Rev. Lett. 85 (2000) 3472−3475, https://doi.org/10.1103/PhysRevLett.85.3472.

[46] K.G. Crawford, D. Qi, J. Mcglynn, T.G. Ivanov, P.B. Shah, J. Weil, A. Tallaire, A.Y. Ganin, D.A.J. Moran, Thermally stable, high performance transfer doping of diamond using transition metal oxides, Sci. Rep. 8 (2018) 3342, https://doi.org/10.1038/s41598-018-21579-4.

[47] V.P. Chechev, N.K. Kuzmenko, Table de Radionucléides − Am-241, 2010. http://www.lnhb.fr/nuclides/Am-241_tables.pdf. (Accessed 21 January 2019).

[48] L.A. Popeko, G.V. Val'skii, D.M. Kaminker, G.A. Petrov, Delayed gamma emission in the fission of 235U, J. Nucl. Energy − Parts A/B React. Sci. Technol. 20 (1966) 811−814, https://doi.org/10.1016/0368-3230(66)90162-5.

[49] K.W. Fornalski, Simple empirical correction functions to cross sections of the photoelectric effect, Compton scattering, pair and triplet production for carbon radiation shields for intermediate and high photon energies, J. Phys. Commun. 2 (2018) 35038, https://doi.org/10.1088/2399-6528/aab408.

[50] J.V. Macpherson, A practical guide to using boron doped diamond in electrochemical research, Phys. Chem. Chem. Phys. 17 (2015) 2935−2949, https://doi.org/10.1039/C4CP04022H.

[51] M.C. James, F. Fogarty, R. Zulkharnay, N.A. Fox, P.W. May, A review of surface functionalisation of diamond for thermionic emission applications, Carbon N. Y. 171 (2021) 532−550, https://doi.org/10.1016/j.carbon.2020.09.019.

[52] R.D. Deslattes, E.G. Kessler Jr., P. Indelicato, L. de Billy, E. Lindroth, J. Anton, J.S. Coursey, D.J. Schwab, J. Chang, R. Sukumar, K. Olsen, R.A. Dragoset, X-ray transition energies database, NIST Stand. Ref. Database 128 (2005), https://doi.org/10.18434/T4859Z.

[53] M. Drakopoulos, T. Connolley, C. Reinhard, R. Atwood, O. Magdysyuk, N. Vo, M. Hart, L. Connor, B. Humphreys, G. Howell, S. Davies, T. Hill, G. Wilkin, U. Pedersen, A. Foster, N. De Maio, M. Basham, F. Yuan, K. Wanelik, I12: the joint engineering, environment and processing (JEEP) beamline at diamond light source, J. Synchrotron Radiat. 22 (2015) 828−838, https://doi.org/10.1107/S1600577515003513.

[54] D.K. Schroder, Semiconductor Material and Device Characterisation, third ed., John Wiley & Sons, Inc., Hoboken, New Jersey, USA, 2006 https://doi.org/10.1002/0471749095.

[55] C.-H. Chiang, C.-G. Wu, Bulk heterojunction perovskite-PCBM solar cells with high fill factor, Nat. Photon. 10 (2016) 196−201, https://doi.org/10.1038/NPHOTON.2016.3.

[56] M. Wang, H. Wang, W. Li, X. Hu, K. Sun, Z. Zang, Defect passivation using ultrathin PTAA layers for efficient and stable perovskite solar cells with a high fill factor and eliminated hysteresis, J. Mater. Chem. A 7 (2019) 26421−26428, https://doi.org/10.1039/c9ta08314f.

[57] I. Haughton, I.L. Paz, M. McGowan, A. Oh, A. Porter, P.S. Salter, O. Allegre, Barrier potential for laser written graphitic wires in diamond, Diam. Relat. Mater. 111 (2020) 108164, https://doi.org/10.1016/j.diamond.2020.108164.

[58] F. Bachmair, L. Bäni, P. Bergonzo, B. Caylar, G. Forcolin, I. Haughton, D. Hits, H. Kagan, R. Kass, L. Li, A. Oh, S. Phan, M. Pomorski, D.S. Smith, V. Tyzhnevyi, R. Wallny, D. Whitehead, A 3D diamond detector for particle tracking, Nucl. Instruments Methods Phys. Res. Sect. A Accel. Spectrometers, Detect. Assoc. Equip. 786 (2015) 97−104, https://doi.org/10.1016/j.nima.2015.03.033.

[59] I. Lopez Paz, O. Allegre, Z. Li, A. Oh, A. Porter, D. Whitehead, Study of electrode fabrication in diamond with a femto-second laser, Phys. Status Solidi 216 (2019) 1900236, https://doi.org/10.1002/pssa.201900236.

[60] B. Caylar, M. Pomorski, P. Bergonzo, Laser-processed three dimensional graphitic electrodes for diamond radiation detectors, Cit. Appl. Phys. Lett. Appl. Phys. Lett. Appl. Phys. Lett 103 (2013), https://doi.org/10.1063/1.4821035.

[61] S. Lagomarsino, M. Bellini, C. Corsi, F. Gorelli, G. Parrini, M. Santoro, S. Sciortino, Three-dimensional diamond detectors: charge collection efficiency of graphitic electrodes, Appl. Phys. Lett. 103 (2013) 233507, https://doi.org/10.1063/1.4839555.

[62] M.J. Booth, G.T. Forcolin, V. Grilj, B. Hamilton, I. Haughton, M. McGowan, S.A. Murphy, A. Oh, P.S. Salter, I. Sudić, N. Skukan, Study of cubic and hexagonal cell geometries of a 3D diamond detector with a proton microbeam, Diam. Relat. Mater. 77 (2017) 137−145, https://doi.org/10.1016/j.diamond.2017.06.014.

[63] M. Girolami, L. Criante, F. Di Fonzo, S. Lo Turco, A. Mezzetti, A. Notargiacomo, M. Pea, A. Bellucci, P. Calvani, V. Valentini, D.M. Trucchi, Graphite distributed electrodes for diamond-based photon-enhanced thermionic emission solar cells, Carbon N. Y. 111 (2017) 48−53, https://doi.org/10.1016/j.carbon.2016.09.061.

[64] A. Hoffman, A. Laikhtman, Photon stimulated desorption of hydrogen from diamond surfaces via core-level excitations: fundamental processes and applications to surface studies, J. Phys. Condens. Matter 18 (2006) 1517−1546, https://doi.org/10.1088/0953-8984/18/30/S08.

[65] C. Verona, W. Ciccognani, S. Colangeli, E. Limiti, M. Marinelli, G. Verona-Rinati, Comparative investigation of surface transfer doping of hydrogen terminated diamond by high electron affinity insulators, J. Appl. Phys. 120 (2016) 25104, https://doi.org/10.1063/1.4955469.

[66] C. Sun, T. Hao, J. Li, H. Ye, C. Gu, The design and performance of hydrogenterminated diamond metal-oxide-semiconductor field-effect transistors with high k oxide HfO2, Micro Nano Eng 6 (2020) 100046, https://doi.org/10.1016/j.mne.2020.100046.

[67] A.H. Compton, A quantum theory of the scattering of X-rays by light elements, Phys. Rev. 21 (1923) 483−502, https://doi.org/10.1103/PhysRev.21.483.

[68] G. Conte, E. Giovine, M. Girolami, S. Salvatori, A. Bolshakov, V. Ralchenko, V. Konov, Polycrystalline diamond UV-triggered MESFET receivers, Nanotechnology 23 (2012) 6, https://doi.org/10.1088/0957-4484/23/7/075202.

[69] S. Agostinelli, J. Allison, K. Amako, J. Apostolakis, H. Araujo, P. Arce, M. Asai, D. Axen, S. Banerjee, G. Barrand, F. Behner, L. Bellagamba, J. Boudreau, L. Broglia, A. Brunengo, H. Burkhardt, S. Chauvie, J. Chuma, R. Chytracek, G. Cooperman, G. Cosmo, P. Degtyarenko, A. Dell 'acqua, G. Depaola, D. Dietrich, R. Enami, A. Feliciello, C. Ferguson, H. Fesefeldt, G. Folger, F. Foppiano, A. Forti, S. Garelli, S. Giani, R. Giannitrapani, D. Gibin, J.J. Gómez Cadenas, I. González, G.G. Abril, G. Greeniaus, W. Greiner, V. Grichine, A. Grossheim, S. Guatelli, P. Gumplinger, R. Hamatsu, K. Hashimoto, H. Hasui, A. Heikkinen, A. Howard, V. Ivanchenko, A. Johnson, F.W. Jones, J. Kallenbach Aa, N. Kanaya, M. Kawabata, Y. Kawabata, M. Kawaguti, S. Kelner, P. Kent, A. Kimura, T. Kodama, R. Kokoulin, M. Kossov, H. Kurashige, E. Lamanna, T. Lampén, V. Lara, V. Lefebure, F. Lei, M. Liendl, W. Lockman, F. Longo, S. Magni, M. Maire, E. Medernach, K. Minamimoto, P. Mora De Freitas, Y. Morita, K. Murakami, M. Nagamatu, R. Nartallo, P. Nieminen, T. Nishimura, K. Ohtsubo, M. Okamura, S. O'neale, Y. Oohata, K. Paech, J. Perl, A. Pfeiffer, M.G. Pia, F. Ranjard, A. Rybin, S. Sadilov, E. Di Salvo, G. Santin, T. Sasaki, N. Savvas, Y. Sawada, S. Scherer, S. Sei, V. Sirotenko, D. Smith, N. Starkov, H. Stoecker, J. Sulkimo, M. Takahata, S. Tanaka, E. Tcherniaev, E. Safai Tehrani, M. Tropeano, P. Truscott, H. Uno, L. Urban, P. Urban, M. Verderi, A. Walkden, W. Wander, H. Weber, J.P. Wellisch, T. Wenaus, D.C. Williams, D. Wright, T. Yamada, H. Yoshida, D. Zschiesche, Geant4—a simulation toolkit, Nucl. Instrum. Methods Phys. Res. A 506 (2003) 250−303, https://doi.org/10.1016/S0168-9002(03)01368-8.

[70] C.J. Werner, J.S. Bull, C.J. Solomon, F.B. Brown, G.W. Mckinney, M.E. Rising, D.A. Dixon, R.L. Martz, H.G. Hughes, L.J. Cox, A.J. Zukaitis, J.C. Armstrong, R.A. Forster, L. Casswell, MCNP Version 6.2 Release Notes, n.d. https://mcnp.lanl.gov/pdf_files/la-ur-18-20808.pdf. (Accessed 16 September 2020).

[71] H. Lee, M.S. Yim, Examination of scintillator-photovoltaic cell-based spent fuel radiation energy conversion for electricity generation, Prog. Nucl. Energy 94 (2017) 46−54, https://doi.org/10.1016/j.pnucene.2016.10.004.

[72] M. Wu, J. Zhang, Design and simulation of high conversion efficiency betavoltaic battery based on a stacked multilayer structure, AIP Adv. 9 (2019), 075124, https://doi.org/10.1063/1.5094826.

[73] N. Rattray Erasmus, Simulation of Silicon and Diamond Detector Systems by GEANT4 Simulation Techniques, University of Western Cape, 2014. http://etd.uwc.ac.za/xmlui/handle/11394/3914.

[74] J.A. Davis, K. Ganesan, A.D. C Alves, S. Guatelli, M. Petasecca, A.A. Jeremy Davis, J. Livingstone, M.L.F. Lerch, D.A. Prokopovich, M.I. Reinhard, R.M. Siegele, S. Prawer, D. Jamieson, Z. Kuncic, V.L. Pisacane, J.F. Dicello, Z. Ziegler, M. Zaider, A.B. Rosenfeld, Characterization of a novel diamond-based microdosimeter prototype for radioprotection applications in space environments, IEEE Trans. Nucl. Sci. 59 (2012) 3110−3116, https://doi.org/10.1109/TNS.2012.2218131.

[75] A. Morozzi, D. Passeri, S. Vecchi, L. Servoli, S. Sciortino, Combined TCAD and Geant4 simulations of diamond detectors for timing applications, Nucl. Instruments Methods Phys. Res. Sect. A Accel. Spectrometers, Detect. Assoc. Equip. 936 (2019) 436−438, https://doi.org/10.1016/j.nima.2018.07.091.

[76] EH300 Datasheet (PDF) - Advanced Linear Devices, (n.d.). https://pdf1.alldatasheet.com/datasheet-pdf/view/206196/ALD/EH300.html. (Accessed 28 July 2020).